ELSEVIER

Remote Sensing of Environment 80 (2002) 203–212

Remote Sensing of Environment

www.elsevier.com/locate/rse

Impact of sensor's point spread function on land cover characterization: assessment and deconvolution

Chengquan Huang[a,*], John R.G. Townshend[a,b], Shunlin Liang[a], Satya N.V. Kalluri[a,1], Ruth S. DeFries[a,c]

[a]Department of Geography, University of Maryland, College Park, MD 20742, USA
[b]Institute for Advanced Computer Studies, University of Maryland, College Park, MD 20742, USA
[c]Earth System Science Interdisciplinary Center, University of Maryland, College Park, MD 20742, USA

Received 9 March 2001; received in revised form 19 July 2001; accepted 21 July 2001

Abstract

Measured and modeled point spread functions (PSF) of sensor systems indicate that a significant portion of the recorded signal of each pixel of a satellite image originates from outside the area represented by that pixel. This hinders the ability to derive surface information from satellite images on a per-pixel basis. In this study, the impact of the PSF of the Moderate Resolution Imaging Spectroradiometer (MODIS) 250 m bands was assessed using four images representing different landscapes. Experimental results showed that though differences between pixels derived with and without PSF effects were small on the average, the PSF generally brightened dark objects and darkened bright objects. This impact of the PSF lowered the performance of a support vector machine (SVM) classifier by 5.4% in overall accuracy and increased the overall root mean square error (RMSE) by 2.4% in estimating subpixel percent land cover. An inversion method based on the known PSF model reduced the signals originating from surrounding areas by as much as 53%. This method differs from traditional PSF inversion deconvolution methods in that the PSF was adjusted with lower weighting factors for signals originating from neighboring pixels than those specified by the PSF model. By using this deconvolution method, the lost classification accuracy due to residual impact of PSF effects was reduced to only 1.66% in overall accuracy. The increase in the RMSE of estimated subpixel land cover proportions due to the residual impact of PSF effects was reduced to 0.64%. Spatial aggregation also effectively reduced the errors in estimated land cover proportion images. About 50% of the estimation errors were removed after applying the deconvolution method and aggregating derived proportion images to twice their dimensional pixel size.

1. Introduction

Mapping land cover using remotely sensed images most commonly involves using the reflectances or radiances of each pixel to assign it to one of a number of land cover classes. The assumption is made that the information content of a pixel originates solely from within its footprint. In an actual remotely sensed image, however, a substantial portion of the spectral signal of each pixel comes from surrounding areas (Forster & Best, 1994; Townshend, 1981). This is a consequence of many factors including the optics of the instrument, the detector and electronics, atmospheric effects, as well as image resampling (Markham, 1985; Schowengerdt, 1997). These effects are described either by the point spread function (PSF), which characterizes a sensor's response to point signals, or alternatively by its Fourier transform, the optical transfer function (Williams & Becklund, 1989). Such effects constitute an inherent source of uncertainty in satellite images because signals from beyond a pixel's area will contribute to the value assigned to it. For example, it has been estimated that less than half of the signal recorded by the Landsat's first Multispectral Scanner System originates from the pixel itself (Townshend, 1981).

A previous study demonstrated the impact of PSF effects on the estimation of land cover proportions based on an analysis of a simplified landscape using linear mixture modeling (Townshend et al., 2000). In this simplified landscape, actual boundaries of land cover units were used, but all pixels of each cover type were assigned to the mean signature of that

* Corresponding author. Raytheon Systems Corporation, USGS/EROS Data Center, Sioux Falls, SD 57198, USA. Tel.: +1-605-594-6817; fax: +1-605-594-6529.

E-mail address: huang@usgs.gov (C. Huang).

[1] Current affiliation: Raytheon Systems Corporation, Lanham, MD, USA.

0034-4257/01/$ – see front matter
PII: S0034-4257(01)00298-X

cover type, resulting in an image consisting solely of pure pixels at 30-m resolution. The 30-m pixels were then aggregated to 250-m pixels, giving a landscape of exactly known pixel proportions. The standard error of estimation (SEE) in predicted subpixel land cover proportion, which would be 0% without the impact of the PSF (Kalluri et al., 1997), was found to be 6.69%. A combination of deconvolution and aggregation of pixel values reduced the SEE to 1.36%.

In this paper, we have quantified the impact of the PSF on remote sensing images of real landscapes using a PSF model of the Moderate Resolution Imaging Spectroradiometer (MODIS), and have tested the effectiveness of a deconvolution method. We first give a description of the deconvolution method and then the experimental design of this study. The PSF model and the deconvolution were assessed of their impacts on image quality, land cover classification, and subpixel land cover estimation.

2. The MODIS PSF model and deconvolution method

The PSF can be modeled as a function $\mathrm{PSF}(u, v, x, y)$ that maps an input pattern $g(u, v)$ in the object space into an output pattern $R(x, y)$ in the image space (Williams & Becklund, 1989):

$$R(x,y) = \iint \mathrm{PSF}(x-u, y-v) g(u,v) \mathrm{d}u \mathrm{d}v \qquad (1)$$

According to the design specifications, the PSF of MODIS 250 m bands can be modeled as a circularly symmetric Gaussian-like shape using the following function (Barker & Burelhach, 1992):

$$\mathrm{PSF}(x,y,u,v) = \exp\left(-\frac{(x-u)^2 + (y-v)^2}{2\sigma^2}\right) \qquad (2)$$

where x and y are the cross- and along-track coordinates of a pixel in the image space and u and v the cross- and along-track coordinates in the object space. The pixel size of the sensor is determined by σ, which is 123.5 m for the 250-m bands (Barker & Burelhach, 1992). Laboratory measurements of the sensor's PSF were very close to the specifications (Barnes, Pagano, & Salomonson, 1998). Though the actual PSF as would be measured from an orbiting satellite should be more complex due to many factors, this model is an ideal example for illustrating the impact of an actual PSF and proving the concept of partially deconvolving such impact based on a known PSF model.

Because we wanted to compare the use of 250-m resolution data with and without the impact of the PSF, it was more convenient to use TM data at 30-m resolution to simulate 250-m pixels than to use MODIS data itself. Given the transfer function of Landsat Thematic Mapper (TM) (Markham, 1985), a filter was defined to simulate MODIS data from TM image according to the above PSF model (Barker & Burelhach, 1992). To avoid dealing with partial TM pixels, the size of a simulated MODIS pixel was defined to be 256.5 m in both scan and track directions, nine times that of a TM pixel in one dimension (Fig. 1). This adjustment should not affect the general conclusions on the impact of the PSF and the effectiveness of the deconvolution method because it did not change the relative responses of the sensor to neighboring pixels.

2.1. The deconvolution method

Fig. 1 illustrates how pixel values can be affected by the impact of an actual PSF. Ideally, the signal of a pixel would be solely derived from within that pixel using an ideal PSF having a uniform response to signals from within that pixel and no response to signals from outside that pixel. A PSF with this attribute will be referred to as the *ideal PSF* throughout this paper, though we recognize that there will be some small PSF effects present from TM data and from atmospheric effects (see below). The actual PSF model, however, shows that the sensor not only responds to radiance from within that pixel, but also to that from surrounding pixels. For an orbiting sensor, such adjacency effect can be more significant due to atmospheric effects and off nadir view geometry, and likely will be different in the along- and cross-track directions. Nevertheless, we will refer to the "actual PSF" model shown in Fig. 1 as the *actual PSF* throughout this paper to distinguish it from the ideal PSF.

In order to reduce the impact of PSF effects, it is necessary to invert the radiance derived using the ideal PSF from that derived using the actual PSF. A straightforward method is to invert the PSF and apply it to the image to be deconvolved. This procedure can also be performed in the frequency domain using a Wiener filter (e.g., Fales, Huck, McCormick, & Park, 1988). This method, however, may enhance noises in the image being deconvolved (Frieden, 1980). While some efforts have been made to deal with this problem in the space domain using iterative algorithms

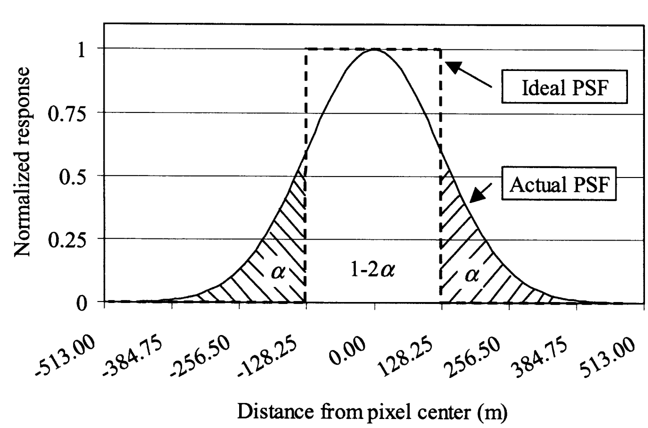

Fig. 1. The actual and ideal PSFs for simulating MODIS data from TM images. The PSFs are the same for both scan and track directions. The integrated response of the actual PSF to a neighboring pixel normalized by its overall response in one dimension is represented by α.

Table 1
TM images for assessing the impacts of the PSF and the effectiveness of the deconvolution method

Location	Path	Row	Date	Major land use/ land cover types
Maryland, USA	015	033	August 14, 1985	Agriculture/ Forest/Urban
Al Buhayrah, Egypt	177	038	June 7, 1984	Desert/ Agriculture
Santa Cruz, Bolivia	230	072	July 2, 1986	Tropical forest
Ontario, Canada	020	026	October 20, 1985	Boreal forest

(e.g., Frieden, 1980; Meinel, 1986), we found that after the weighting factors of the PSF were adjusted slightly, the inversion method could partially deconvolve the impact of the PSF without introducing excessive noise.

Considering the resolution limitation of a given sensor system, we represent the PSF model of Eq. (2) in a discrete format. According to Fig. 1, only immediately neighboring pixels have substantial contributions to the recorded radiance of a pixel. Let α be the integrated response of the sensor to radiance from an immediately neighboring pixel normalized by the overall response in one dimension (the shaded area of Fig. 1), which is 0.1464 according to Eq. (2). The PSF in the two-dimensional space can be written as:

$$\mathrm{PSF}(\alpha) = \begin{bmatrix} \alpha \\ 1-2\alpha \\ \alpha \end{bmatrix} (\alpha \quad 1-2\alpha \quad \alpha)$$

$$= \begin{bmatrix} \alpha^2 & \alpha(1-2\alpha) & \alpha^2 \\ \alpha(1-2\alpha) & (1-2\alpha)^2 & \alpha(1-2\alpha) \\ \alpha^2 & \alpha(1-2\alpha) & \alpha^2 \end{bmatrix} \tag{3}$$

This representation of the PSF assumes that the sensor's response is uniform within each neighboring pixel. While this is not accurate, it is a close and necessary approximation because the spatial variation of radiance within each pixel is unknown. With this assumption, and rewriting the 3×3 matrix in Eq. (3) as $\{\mathrm{PSF}_{i,j}(\alpha)\}$, $i,j = 1, 2, 3$, the following relationship exists between the radiance derived using the ideal filter (r) and that derived using the PSF filter (R) for each pixel (p,l) except the edge of the whole image:

$$R_{p,l} = \sum_{i=-1}^{1} \sum_{j=-1}^{1} \mathrm{PSF}_{i+2,j+2}(\alpha) r_{p+i,l+j},$$

$$p = 2, \ldots, M-1 \text{ and } l = 2, \ldots, N-1 \tag{4}$$

where M and N are the number of pixels and lines of an image. The boundary conditions for applying Eq. (4) to the edge pixels of the whole image can be defined in many ways. We expanded the entire image by one pixel in all four directions by replicating the edge pixels. This gave the same number of unknown variables and equations, and $r_{p,l}$ was inverted from $R_{p,l}$ by solving Eq. (4).

It should be noted that for a full satellite image, there could be millions of equations in Eq. (4). Solving such a huge equation group is computationally very expensive. Fortunately, Eq. (4) is a sparse linear system and may be handled efficiently using some special techniques (Press, Teukolsky, Vetterling, & Flannery, 1992). In this study, we used the "solve" routine of Splus to demonstrate this deconvolution approach. The "solve" routine implements several standard methods for solving linear equation groups (Chambers & Hastie, 1992).

3. Data and experimental design

The imaging process described in Eq. (1) shows that the impact of the PSF not only depends on the PSF itself, but also on the spatial variability of the input pattern. In large homogeneous areas, images derived using the actual PSF may not be significantly different from those derived using the ideal one. However, in heterogeneous regions with strong contrast among neighboring areas, differences between images derived using the two PSFs can be quite significant. In this assessment, four TM images representing different landscapes were used, each covering an area of 16.5 × 16.5 km (Table 1).

To ensure compatibility of the results from different area, the digital number (DN) of each image was converted to a top-of-atmospheric reflectance using the procedure of Markham and Barker (1986). The reflectance images were then degraded using the actual and ideal PSFs given in Fig. 1, respectively. For simplicity, the resultant images are referred to as the "convolved" and "ideal" images through the rest of the paper. Because the ideal images were derived from TM images, they were affected by the TM's PSF.

Table 2
Impact of the PSF on the standard deviation (S.D.) of images

Location of image	$\mathrm{S.D.}_{\cdot\mathrm{convolved}}$ (reflectance %)	$\mathrm{S.D.}_{\cdot\mathrm{ideal}}$ (reflectance %)	$\mathrm{S.D.}_{\cdot\mathrm{ideal}}$ reduced (%)
MODIS band 1			
Maryland, USA	1.13	1.22	7.64
Al Buhayrah, Egypt	5.58	5.78	3.37
Santa Cruz, Bolivia	0.40	0.45	9.76
Ontario, Canada	0.39	0.48	17.37
MODIS band 2			
Maryland, USA	5.97	6.18	3.36
Al Buhayrah, Egypt	4.06	4.23	4.16
Santa Cruz, Bolivia	0.65	0.74	12.09
Ontario, Canada	2.29	2.52	9.13

The subscript "ideal" refers to images derived using the ideal PSF shown in Fig. 1. The last column shows the percentage of the standard deviation of the images derived using the ideal PSF ($\mathrm{S.D.}_{\cdot\mathrm{ideal}}$) reduced when the images were derived using the actual PSF ($\mathrm{S.D.}_{\cdot\mathrm{convolved}}$).

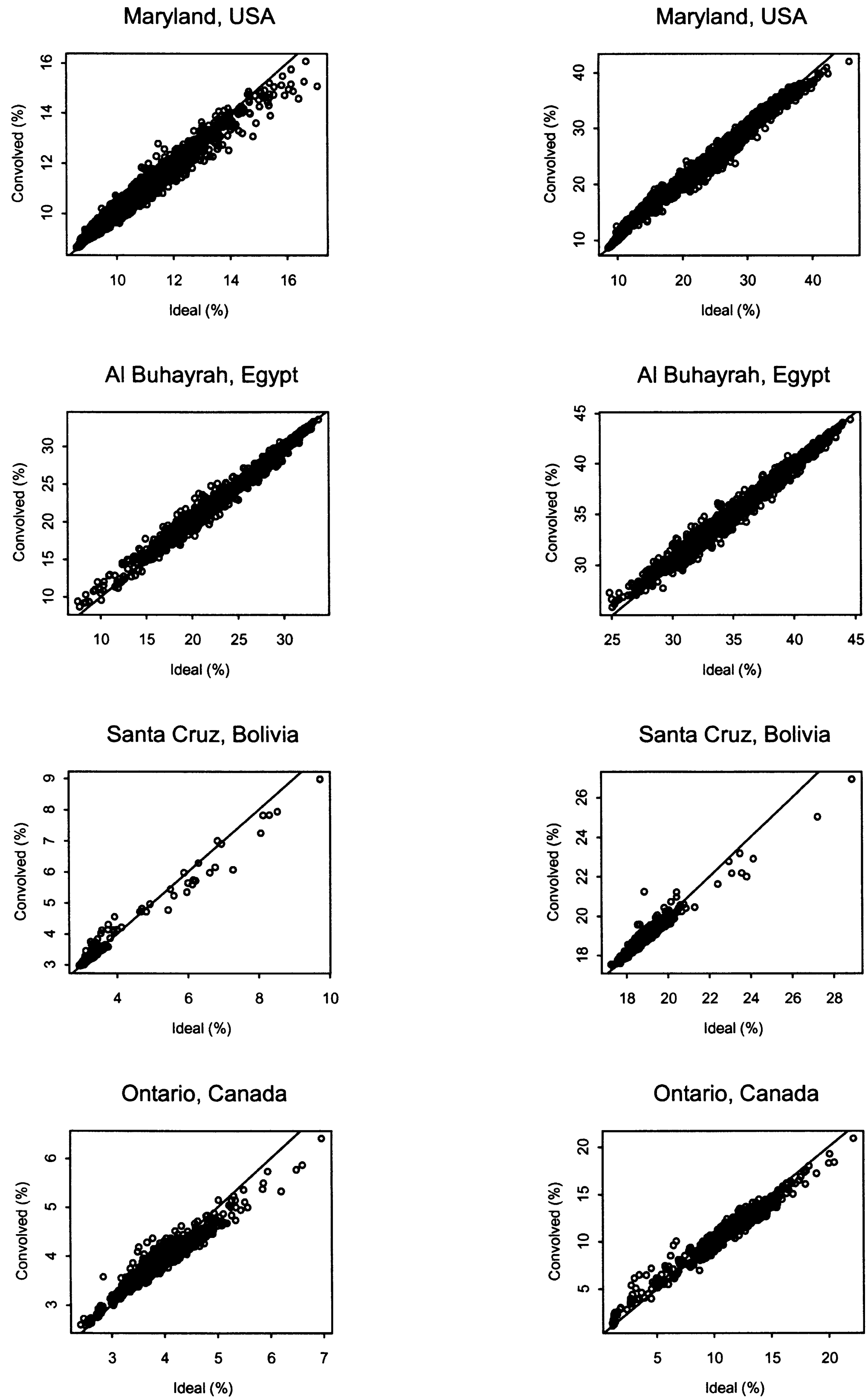

Fig. 2. Impact of PSF effects shown as the differences between the convolved images and the ideal ones (i.e., those derived using the ideal PSF). The units for both the x and y axis are percent reflectance (%). Plots in the left side are for the red band and those in the right side are for the near infrared band.

However, such impacts should be negligible at 256.5-m resolution because most of them cancel one another when the 28.5-m pixels were aggregated to 256.5 m. Applying the deconvolution method described above to the convolved images (see Eq. (4)) partially deconvolved them. Differences between the convolved images and the ideal ones can be attributed to the impacts of the PSF, while those between the partially deconvolved images and the ideal ones indicate the residual impact of the PSF on the partially deconvolved images. Improvements of the partially deconvolved images over the convolved ones reflect the effectiveness of the deconvolution method.

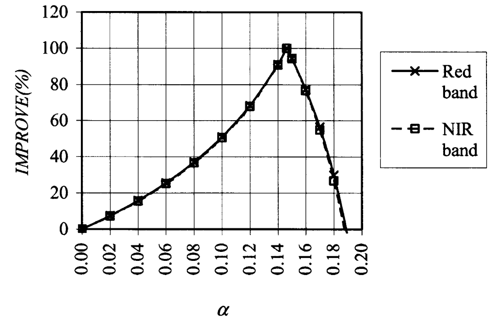

Fig. 4. Different impacts of underestimation (when $\alpha < 0.1464$) and overestimation (when $\alpha < 0.1464$) by the deconvolution method of signals originating from neighboring pixels on the performance of this method. In order to separate overestimation from underestimation, the spatial heterogeneity within each window of 9×9 TM pixels was removed by setting all pixels within the window to the average value of that window, resulting in a simplified TM image. The actual PSF was then applied to this simplified TM image and a simplified MODIS image was created. When the deconvolution method was applied to this simplified MODIS image, for each and every pixel in this image, the amount of signal derived from surrounding areas was accurately estimated using Eq. (9) when α was set to 0.1464, underestimated when α was less than 0.1464, and overestimated when α was greater than 0.1464. The initial increase in performance as α increased from 0 to 0.1464 was solely due to the decrease of underestimation errors, while the decrease in performance as α exceeded 0.1464 was solely due to the increase of overestimation errors. IMPROVE is defined in Eq. (7).

4. PSF impact on image quality and its deconvolution

4.1. Impact on image quality

The PSF affects image quality in several ways. First, because the actual PSF includes signals from an area larger than an individual pixel, it smoothens surface variability more severely than the ideal PSF. As a result, the convolved image derived using the actual PSF should have less spatial variability than an ideal one derived using the ideal PSF. Table 2 shows that for the red and NIR bands of all four test areas, the convolved images had between 3% and 17% smaller standard deviations than the ones without PSF effects.

A pixel derived using the actual PSF likely will have a different value from a pixel derived using the ideal PSF because the former originates from a larger area. Due to uneven weighting factors of the actual PSF, such differences are functions of the relative brightness of neighboring pixels and the spatial arrangement of dark and bright objects within each pixel. Fig. 2 compares the reflectance values of the convolved images with the ideal ones, i.e., those with minimal instrument PSF effects. These plots show that in addition to the pixels being scattered in considerably wide ranges along the 1:1 line, for the convolved images of all four test sites, dark pixels were brighter and bright pixels were less bright when compared to the corresponding pixels in the ideal images.

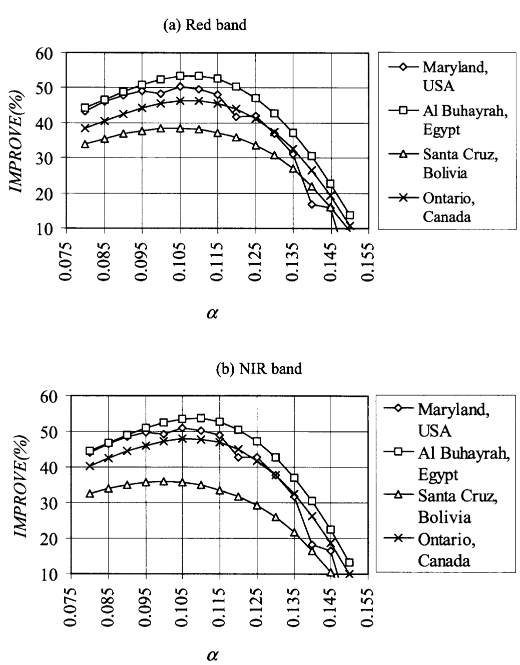

Fig. 3. Performance of the deconvolution method as a function of α. IMPROVE is defined in Eq. (7).

4.2. Tuning the performance of the deconvolution method

In order to measure the performance of the deconvolution method, we quantify the impact of the PSF by the mean absolute difference ($\mathrm{MAD_{PSF}}$) between the convolved image (R_i) and the ideal one (r_i). We also calculate the mean absolute difference ($\mathrm{MAD_{DCV}}$) between the partially deconvolved image ($\mathrm{D}R_i$) and the ideal one to assess the residual impact of the PSF in the partially deconvolved image (Eqs. (5) and (6)):

$$\mathrm{MAD_{PSF}} = \frac{1}{N}\sum_{i=1}^{N} |R_i - r_i| \tag{5}$$

$$\mathrm{MAD_{DCV}} = \frac{1}{N}\sum_{i=1}^{N} |\mathrm{D}R_i - r_i| \tag{6}$$

where N is the number of pixels in the image. The performance of the deconvolution method is measured by

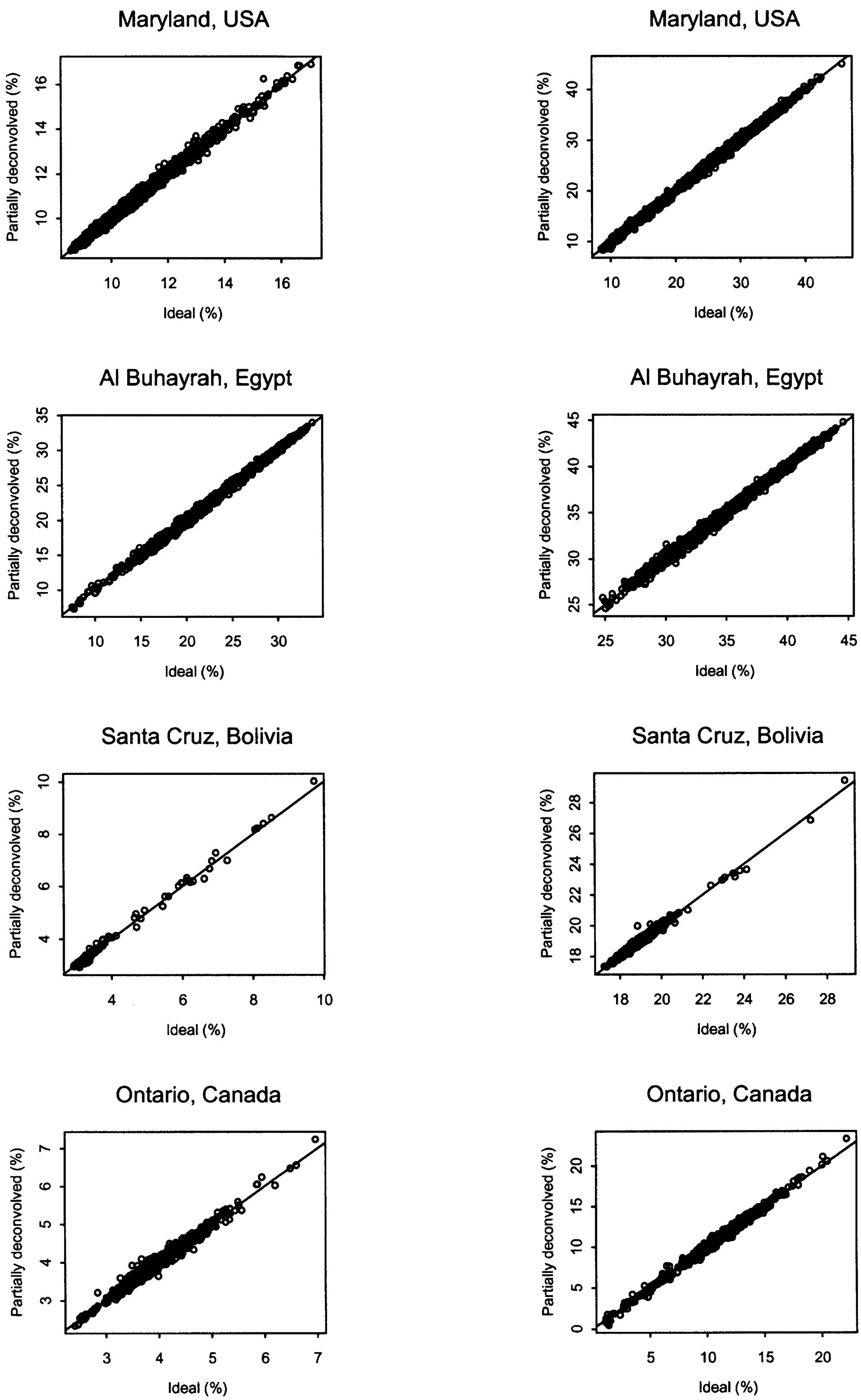

Fig. 5. Residual impact of PSF effects on the partially deconvolved images. The units for both the x and y axes are percent reflectance (%). Plots in the left side are for the red band and those in the right side are for the near infrared band.

Table 3
Deviations of convolved (MAD_{PSF}) and partially deconvolved images (MAD_{DCV}) from ideal ones (i.e., those derived using the ideal PSF) as measure by the mean absolute difference and improvements (IMPROVE) brought by the deconvolution method

Location of image	MAD_{PSF} (reflectance %)	MAD_{DCV} (reflectance %)	IMPROVE (MAD_{DCV} %)
MODIS band 1			
Maryland, USA	0.152	0.075	50.36
Al Buhayrah, Egypt	0.462	0.214	53.65
Santa Cruz, Bolivia	0.031	0.022	34.91
Ontario, Canada	0.101	0.053	47.86
MODIS band 2			
Maryland, USA	0.505	0.243	51.88
Al Buhayrah, Egypt	0.419	0.223	46.70
Santa Cruz, Bolivia	0.118	0.069	41.11
Ontario, Canada	0.337	0.175	48.15

the percentage of the MAD_{PSF} removed by the deconvolution method:

$$\mathrm{IMPROVE} = \frac{\mathrm{MAD_{PSF}} - \mathrm{MAD_{DCV}}}{\mathrm{MAD_{PSF}}} \times 100\% \tag{7}$$

Deconvolving the impact of the PSF requires solving equation group Eq. (4), the coefficients of which were derived from α—the sensor's integrated response to signals from a neighboring pixel in one dimension. Intuitively, the signals originating from neighboring pixels would be most accurately accounted for by equation group Eq. (4) when α equals its modeled value, which is 0.1464 according to the PSF model defined by Eq. (2). However, for all four test images, the deconvolution method performed poorly when α was set to that value (Fig. 3). For both the red and NIR bands of the four test images, the proportion of the PSF's impact removed by the deconvolution method increased as α decreased, and reached a maximum when α was around 0.105. Further decreases in α gave decreased performances.

That the deconvolution method achieved best performances when α was set to 0.105 rather than its modeled value can be attributed to the inability of the deconvolution method to accurately estimate the contributions of surrounding areas for every pixel. According to Eq. (1), the actual contribution of a neighboring pixel i in the input space (u, v) to pixel j in the image space (x, y) should be calculated as:

$$\iint_{\text{pixel } j} \left(\iint_{\text{pixel } i} h(x-u, y-v) g(u,v) \mathrm{d}u\mathrm{d}v \right) \mathrm{d}x\mathrm{d}y \tag{8}$$

Because the input pattern $g(u, v)$ is unknown beyond a sensor's resolving power, Eq. (8) is approximated using the following formula in the deconvolution equation group Eq. (4):

$$\mathrm{PSF}_{i,j}(\alpha) r_i = \iint_{\text{pixel } j} \left(\iint_{\text{pixel } i} h(x-u, y-v)\, \mathrm{d}u\mathrm{d}v \right) \times \mathrm{d}x\mathrm{d}y \iint_{\text{pixel } i} \mathrm{g(u,v)dudv} \tag{9}$$

For each pair of pixel i and j, the difference between Eqs. (8) and (9) is a function of α and the spatial arrangement of dark and bright objects within pixel i. Due to the uneven weighting nature of $h(x-u,y-v)$, Eq. (8) tends to be underestimated by Eq. (9) when brighter objects in pixel i are located near pixel j, but overestimated when darker objects are located near pixel j. The overall amounts of underestimation and overestimation of Eq. (8) by Eq. (9) for an entire image are functions of α. When α increases, the first part decreases while the second part increases. Statistically, the contributions of neighboring pixels are best estimated when the sum of underestimates and overestimates is minimized, which would be achieved when α equals its modeled value—0.1464. The deconvolution would achieve its best performance at this value, if overestimation and underestimation of Eq. (8) by Eq. (9) had the same effect on the performance of the deconvolution method. However, because the inverted matrix of the PSF enhances noises (Forster & Best, 1994; Frieden, 1980), the performance of the deconvolution method degrades more rapidly due to overestimates than due to underestimates of Eq. (8) by Eq. (9). Fig. 4 shows that improvement brought by the deconvolution method decreases more rapidly when overestimates increase than when underestimates increase. Thus, when α increases to around 0.1464, though increases in overestimation are approximately balanced by decreases

Table 4
Performances of the SVM on the convolved, partially deconvolved, and ideal images of the Maryland, USA test site

Source images	Per-class agreement with reference map (pixel): Closed forest	Open forest	Woodland	Nonforest land	Land–water mix	Water	Overall accuracy (%)
Convolved image	1154	529	316	607	189	291	75.34
Partially deconvolved image	1206	578	341	620	196	298	79.08
Ideal image	1215	614	348	630	200	300	80.74
Number of pixels in the reference map	1342	782	626	824	219	303	100.00

in underestimation, the impact of increased overestimation on the performance of the deconvolution method exceeds that of decreased underestimation. As a result, the net effectiveness of the deconvolution method reaches its peak value before α reaches its modeled value.

4.3. Effectiveness of the deconvolution method

The fact that the deconvolution method achieved optimal performances on both the red and NIR bands of all four test images with an α value around 0.105 suggests that regard-

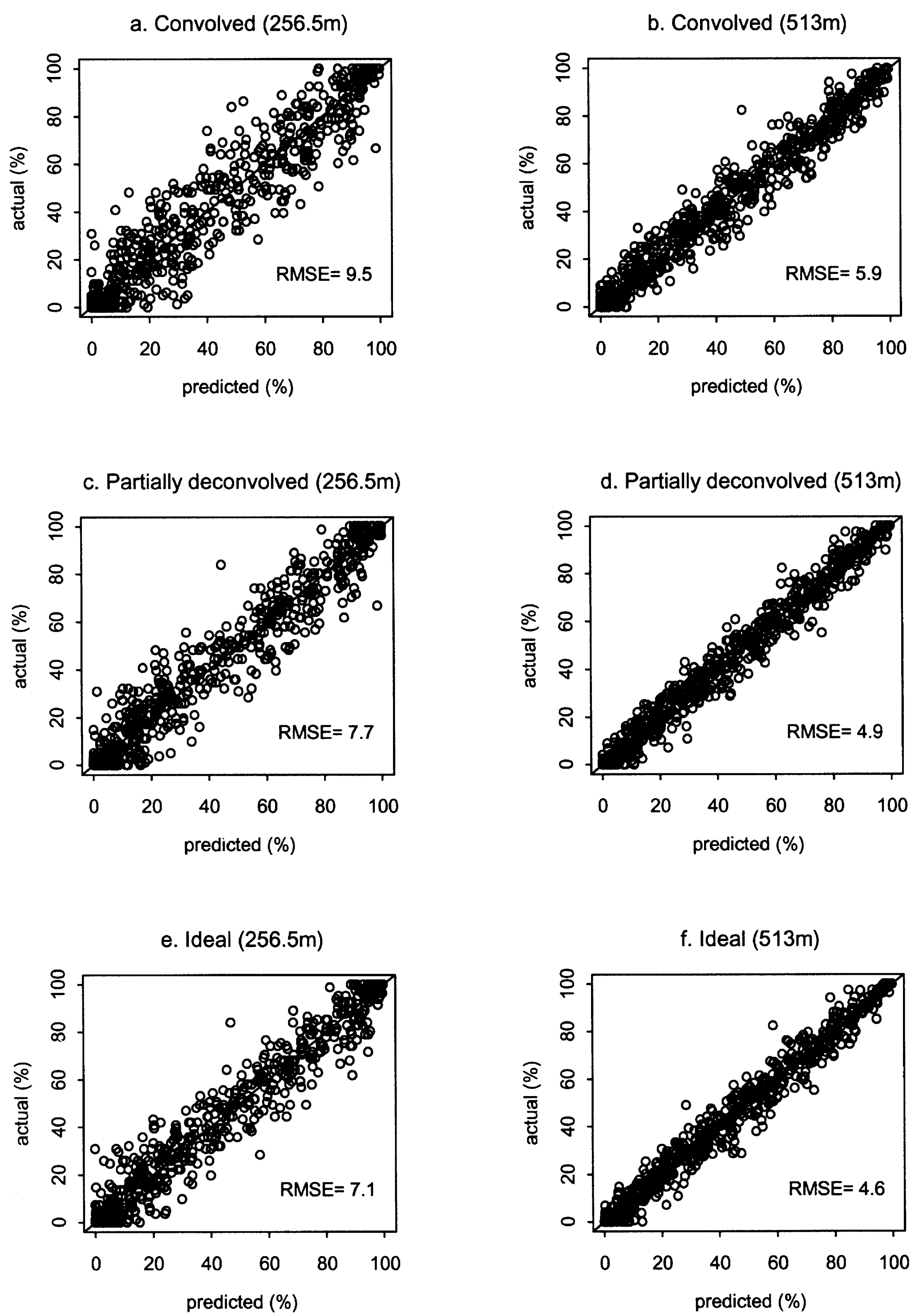

Fig. 6. Impact of the PSF on the estimation of subpixel land cover proportions and improvements brought by the deconvolution method and spatial aggregation. The proportions were estimated from (a) convolved, (c) partially deconvolved, and (e) ideal (i.e., that derived using the ideal PSF) images from the Maryland, USA test site using a SRT method, and were aggregated to 513 m (b, d, and f respectively) through spatial averaging.

less of surface conditions, the impact of a known PSF model may be partially deconvolved using this deconvolution method with a single α value, which was set to 0.105 for the remainder of this study.

Fig. 5 compares the partially deconvolved images to the ideal ones. A comparison of this figure to Fig. 2 shows that not only are the points in these plots much closer to the 1:1 line, but the trends of dark objects being brightened and bright ones being darkened in the convolved image have also been corrected. Table 3 gives quantitative measures of the impact of the actual PSF (MAD_{PSF}) on the four test images, its residual impact (MAD_{DCV}) after the deconvolution method was applied, and the improvements (IMPROVE) brought by the deconvolution method. The deconvolution method removed more than 40% of the impact of the actual PSF on all images except the red band of the Santa Cruz, Bolivia image. The relatively smaller improvement brought by the deconvolution method to this image was probably because this image had relatively uniform and very low signals. The relative noise enhancement of this deconvolution method on such images tends to be higher than on brighter and more heterogeneous images.

5. Implications for land cover characterization

In order to evaluate the consequences of the impact of the actual PSF and the deconvolution method on land cover characterization, classifications and estimations of subpixel land cover proportions were carried out on the convolved, partially deconvolved, and ideal images. This was carried out for the Maryland, USA test site, where wall-to-wall reference land cover maps for training and validation purposes had been collected through field work.

The classifications were derived using a support vector machine (SVM) classifier (Vapnik, 1995). The computer program of this classifier, SVM^{light}, was developed by Joachims (1998). Subpixel land cover proportions were derived using a stepwise regression tree (SRT) method (Huang & Townshend, in press). Both algorithms were trained using 20% of the pixels randomly sampled from the Maryland, USA data set. The remaining 80% pixels were used as test pixels in accuracy assessment. The SVM and SRT have been found in previous studies to be more accurate than commonly available alternatives (Huang, Davis, & Townshend, in press; Huang & Townshend, in press).

Table 4 gives the overall accuracies and per-class agreements between the reference map and classifications developed from the convolved, partially deconvolved, and ideal images. For all six land cover classes, the classifications from both the ideal and partially deconvolved images had higher per-class agreements with the reference map than that from the convolved image. As a result, the overall accuracies of classifications developed from the ideal and partially deconvolved image were 5.40% and 3.74% higher than that of the classification developed from the convolved image.

The accuracy of the estimate of the subpixel land cover proportions was measured using the root mean square error (RMSE) of predicted proportions ($\hat{y}_i$) measured against the reference proportions (y_i) (Eq. (10)).

$$\mathrm{RMSE} = \sqrt{\frac{1}{N}\sum_{i=1}^{N}(\hat{y}_i - y_i)^2} \tag{10}$$

Fig. 6 compares the subpixel proportions predicted from the convolved, partially deconvolved and ideal images to the reference proportions and gives the RMSEs. The RMSE was 7.1% when proportions were predicted from the ideal image, i.e., image with minimal PSF effects (Fig. 6e). It increased in absolute terms by 2.4% in percent land cover, when PSF effects were introduced in the convolved image, representing a 35% proportional increase (Fig. 6a). After applying the deconvolution method, the RMSE was only 0.6% greater than that obtained from the ideal image (Fig. 6c).

Previously, we showed in a simulation study (Townshend et al., 2000) that the impact of PSF effects in estimating subpixel land cover proportions could also be reduced simply by aggregating derived proportion images to coarser resolutions. Consequently, we doubled the pixel size to 513 m and aggregated the proportion images by simple spatial averaging. Fig. 6b shows that the estimation error was reduced by more than 40% when we spatially averaged the estimates from the convolved data set. The error was further reduced when the proportion images were derived from the partially deconvolved image and then aggregated (Fig. 6d), slightly higher than that when the proportions were derived from the ideal image and then aggregated (Fig. 6f). Differences between Fig. 6d and f indicate that after applying the deconvolution method and aggregating the proportion images, only 0.3% of the RMSE in absolute value was due to the residual impact of the PSF.

6. Conclusions

The quality of a satellite image and its use for land cover characterization are affected by the PSF of the instrument. An actual PSF generally reduces the spatial variability of satellite images more severely than an ideal PSF, i.e., a spatial averaging filter, and the pixel values derived using the actual PSF will be different from those derived using the ideal one. Using a PSF model of the MODIS 250 m bands as an example, convolved images derived using this model had up to 17% smaller standard deviations than the ideal ones, i.e., images with minimum instrument PSF effects derived using the ideal PSF. Though the mean absolute differences (MAD) in reflectance between the convolved images and the ideal ones were small, on the average, less than 0.5%, most dark objects in the convolved images were brighter than those in the ideal images while bright objects in the convolved images were darker than those in the ideal images. Depending on the spatial arrangement of ground objects, such impact of the PSF may vary from image to image, and cannot be deconvolved effectively by simply inverting the PSF. When the PSF was adjusted with lower weighting factors for signals originating from neighboring pixels than those specified by the actual PSF, however, this inversion method reduced the MAD by about 50%. Though this modification was empirically derived, it was found robust for images of different landscapes.

The above impact of instrument PSF resulted in considerable uncertainties in derived land cover products. While a classification derived from the ideal image of the Maryland, USA data set, i.e., the image with minimum PSF effects, had an overall accuracy of 80.74%, the accuracy dropped to 75.34% when the classification was derived from the convolved image. On the same data set, PSF effects increased the RMSE of the estimates of subpixel land cover from 7.1% to 9.5%. Applying the deconvolution method to the convolved image effectively reduced the uncertainties due to the impact of PSF effects in derived land cover products. The overall accuracy of the classification increased from 75.34% to 79.08%, while the RMSE of subpixel land cover proportions decreased from 9.5% to 7.7%. The RMSE was further reduced to 4.9% when the proportion images were spatially aggregated from 256.5 to 513 m.

These results were based on model simulations using a nadir viewing geometry. Due to atmospheric effects and off nadir view geometry, the impact of the PSF of an orbiting sensor likely will be more significant than revealed in this study. An accurate model of instrument PSF as a function of viewing geometry may allow for partial deconvolution of such impact using the developed deconvolution method. Adjacency effect due to the atmosphere, however, are more difficult to deconvolve because the needed data on atmospheric conditions is often unavailable.

This study reinforces earlier investigation based on modeled landscapes that PSF effects on land cover characterization can be considerable. Much of these effects can be reduced using the developed deconvolution method. To achieve a desired performance level the derived land cover products may need to be aggregated to coarser spatial resolutions.

Acknowledgments

The authors acknowledge support from NSF grant BIR9318183 and a contract from the National Aeronautics and Space Administration (NAS596060). We are grateful to the MODIS Science Data Support Team (SDST) for providing the PSF values and the anonymous referees for their comments and suggestions on the first draft of the paper.

References

Barker, J. L., & Burelhach, J. W. (1992). MODIS image simulation from Landsat TM imagery. In: *ASPRS/ACSM/RT 92* (pp. 156–165). Bethesda, Washington, DC: American Society for Photogrammetry and Remote Sensing.

Barnes, W. L., Pagano, T. S., & Salomonson, V. V. (1998). Prelaunch characteristics of the Moderate Resolution Imaging Spectroradiometer (MODIS) on EOS-AM1. *IEEE Transactions on Geoscience and Remote Sensing*, *36*, 1088–1100.

Chambers, J. M., & Hastie, T. J. (1992). *Statistical Models in S*. Pacific. Grove, CA: Wadsworth and Brooks.

Fales, C. I., Huck, F. O., McCormick, J. A., & Park, S. K. (1988). Wiener restoration of sampled image data: end-to-end analysis. *Journal of the Optical Society of America A*, *5*, 300–314.

Forster, B. C., & Best, P. (1994). Estimation of SPOT P-mode point spread function and derivation of a deconvolution filter. *ISPRS Journal of Photogrammetry and Remote Sensing*, *49*, 32–42.

Frieden, B. R. (1980). Statistical models for the image restoration problem. *Computer Graphics and Image Processing*, *12*, 40–59.

Huang, C., Davis, L. S., & Townshend, J. R. G. (2001). An assessment of support vector machines for land cover classification. *International Journal of Remote Sensing* (in press).

Huang, C., & Townshend, J. R. G. (2001). A stepwise regression tree for nonlinear approximation: applications to estimating subpixel land cover. *International Journal of Remote Sensing* (in press).

Joachims, T. (1998). Text categorization with support vector machines—learning with many relevant features. In: *European Conference on Machine Learning* (pp. 137–142). Chemnitz, Springer, Berlin, Germany.

Kalluri, S. N. V., Huang, C., Mathieu-Marni, S., Townshend, J. R. G., Yang, K., & Chellapa, R. (1997). A comparison of mixture modeling algorithms and their applicability to the MODIS data. In: *IGARSS'97, Singapore* (pp. 171–173). Piscataway, NJ: Institute of Electrical and Electronics Engineers Inc.

Markham, B. L. (1985). The Landsat sensors' spatial responses. *IEEE Transactions on Geoscience and Remote Sensing*, *GE-23*, 864–875.

Markham, B. L., & Barker, J. L. (1986). Landsat MSS and TM post-calibration dynamic ranges, exoatmospheric reflectances and at-satellite temperatures. *EOSAT Landsat Technical Notes*, *1*, 3–8.

Meinel, E. S. (1986). Origins of linear and nonlinear recursive restoration algorithms. *Journal of the Optical Society of America A*, *3*, 787–799.

Press, W. H., Teukolsky, S. A., Vetterling, W. T., & Flannery, B. P. (1992). *Numeric recipes in C: the art of scientific computing*. Cambridge: Cambridge University Press.

Schowengerdt, R. A. (1997). *Remote sensing: models and methods for image processing*. San Diego: Academic Press.

Townshend, J. R. G. (1981). Spatial resolution of satellite images. *Progress in Physical Geography*, *5*, 33–55.

Townshend, J. R. G., Huang, C., Kalluri, S. N. V., DeFries, R. S., Liang, S., & Yang, K. (2000). Beware of per-pixel characterization of land cover. *International Journal of Remote Sensing*, *21*, 839–843.

Vapnik, V. N. (1995). *The nature of statistical learning theory*. New York: Springer.

Williams, C. S., & Becklund, O. A. (1989). *Introduction to the optical transfer function*. New York: Wiley.